Maximizing the capacity of graded-index multimode fibers in the linear regime

Filipe M. Ferreira, *Senior Member, IEEE*, Fabio A. Barbosa, *Member, IEEE*

***Abstract*—In this paper, we investigate the design of multimode fibers (MMFs) guiding over 1000 spatial modes. A trench-assisted graded-index core profile is optimized for low differential mode delay (DMD) over the C-band. The optimization results show that for a maximum DMD of 250 ps/km as much as 400 spatial modes can be supported ideally. It is shown that the optimized DMD scales with the number of modes before it reaches a plateau for a given core-cladding contrast – indicating that maximizing the core radius can allow to increase spatial cardinality without significant delay spread increase. Closed-form equations for optimal refractive-index profile parameters are introduced. The throughput supported by the optimized fibers is studied and the scaling trend with the number of guided modes is analyzed for increasing core-cladding contrast. Throughput is shown to be significantly impacted by Rayleigh scattering, macro-bend loss and coating loss, introducing a practical limit to the scaling of the number of modes – at approximately 1000 spatial modes. Here dubbed as the half-mode number, it corresponds to the number of modes beyond which the extra throughput per additional mode decays to half of that of the best mode. Finally, the impact of the fabrication margins on the DMD of the optimized profiles is analyzed.**

***Index Terms*—Multimode fibers, Differential Mode Delay, Refractive Index Profile.**

I. Introduction

Space-division multiplexing (SDM) has emerged as a solution to overcome the capacity limit of single-mode fibers (SMFs) [1]. Among the possible SDM approaches, multimode fibers (MMFs) [2-5] offer the highest spatial information density followed by coupled-core multi-core fibers (MCFs) [6-9]. Spatial density plays a critical role in maximizing opportunities for opto-electronic integration gains, and transceiver-specific integration is key to the overall value proposition of SDM. Namely, spatial super-channels can share one laser for N spatial tributaries and thus share common digital signal processing (DSP) functions such as laser frequency/phase recovery [10]. Also, with all crosstalk spatial paths originating and terminating at the same transceiver, crosstalk cancellation techniques such as multiple-input multiple-output (MIMO)-DSP [11, 12] can be used.

Despite the potential advantages offered by multimode SDM, it also presents major challenges. The multitude of spatial modes brings new linear impairments, namely group delay (GD) spread [13-18], stemming from the interplay between differential mode delay (DMD) and linear mode coupling (LMC), and mode dependent loss (MDL) [12]. The GD spreading can be overcome using MIMO equalization [11, 12] with complexity scaling by the total delay spread, while MDL introduces a fundamental loss of information throughput. To reduce the GD spreading, multimode SDM fibers are designed with a graded-index core, and, to reduce the macro-bend loss (MBL) of the higher-order modes, a cladding trench is introduced [19, 20]. However, to increase the number of modes supported, higher levels of DMD and MDL must be tolerated as it will be shown further on.

Recent research on MCFs and MMFs has led to significant transmission throughput increase. For short-reach systems at 850 nm, new types of multimode fiber increasing bandwidth several-fold have been demonstrated: a multicore multimode fiber formed from a large number of single mode cores [3] or a larger core graded-index multimode fibers [21]. For high-capacity SDM systems at ~1.55 μm, there has been significant progress on coupled-core MCFs with near-zero modal dispersion [8, 9, 22] up to 19 cores and on rescaled standard graded-index-core MMFs [23, 24] up to 55 spatial modes. Here, we extend the latter approach to a much larger number of modes (up to 1000 spatial modes – twice as many polarization modes) by scaling the core-cladding contrast and the core radius within a 125 μm cladding. The impact of scaling these two parameters on the macro-bend loss (MBL) [25], the Rayleigh scattering loss [26] and the coating loss [27] is systematically studied and the trade-offs identified. We will establish a bound on the number of spatial tributaries that in principle can be efficiently transmitted over a graded-index single-core fiber – this bound being defined as the *number of modes after which throughput per mode decays to half of that of the best mode*, dubbed here as *the half-mode number*.

The paper is organized as follows. Section II describes the profile considered and provides an analysis of the impact of its parameters on DMD and MBL. Section III presents the optimization function and algorithm being used and discusses the optimized profile characteristics. It is shown that over 400 spatial modes can be supported within a $DMD < 250$ ps/km mask typical of OM fibers [28]. Closed-form expressions for profile parameters with optimized DMD are introduced,

This work was supported by the UKRI Future Leaders Fellowship MR/T041218/1. To access the underlying data for this publication, see: https://doi.org/10.5522/04/22574791.

F. M. Ferreira and F. A. Barbosa are with the Department of Electronic and Electrical Engineering at University College London, UK (f.ferreira@ucl.ac.uk).

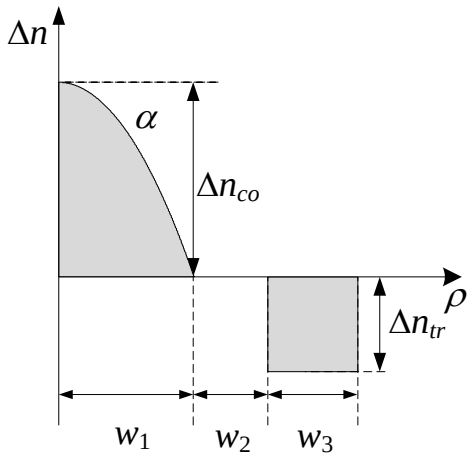

Fig. 1. Refractive index relative difference for a trench-assisted graded-index core profile.

function of the core-cladding contrast and of the core radius. Section IV presents the analysis of the throughput for the optimized fibers given by MIMO theory and the water filling algorithm. It is shown that the throughput scaling with the number of modes can significantly deviate from an otherwise linear growth due to the MDL. Section V studies the impact of fabrication margins on the DMD of the optimized profiles. Section VI summarizes the main conclusions of this paper.

II. Fiber Profile Description and Analysis

In this work, a refractive-index profile composed by a graded-index core and a cladding trench is optimized to reduce modal dispersion and mode-dependent loss and maximize information throughput for an increasing number of guided modes. Fig. 1 presents a schematic of such a profile. There are 6 parameters available for optimization: the core grading exponent, α, the refractive index relative difference at the core and trench, Δn_{co} and Δn_{tr}, respectively, the core radius, w_1, the trench to the core distance, w_2, and the trench width, w_3. The refractive-index profile as a function of the radial coordinate ρ is analytically described by:

$$n(\rho)=\begin{cases} n(0)\sqrt{1-2\Delta n_{co}\left(\frac{\rho}{w_1}\right)^{\alpha}}, & |\rho|<w_1 \\ n_{cl}, & w_1\le|\rho|<w_1+w_2 \\ n_{cl}/\sqrt{1-2\Delta n_{tr}}, & w_1+w_2\le|\rho|<w_1+w_2+w_3 \\ n_{cl}, & |\rho|\ge w_1+w_2+w_3 \end{cases} \quad (1)$$

The refractive index relative difference (Δn) in Fig.1 can be found by replacing $n(\rho)$ in $\Delta n(\rho) = [n^2(\rho) - n_{cl}^2]/[2n^2(\rho)]$, where n_{cl} is the cladding refractive index – assumed to be pure silica.

For a given parameter vector $pv = [\alpha, \Delta n_{co}, \Delta n_{tr}, w_1, w_2, w_3]$, the guided modes and their characteristics are calculated using the vector finite difference mode solver developed in [29] considering the Sellmeier coefficients provided in [30]. In this way, finding for each linearly polarized (LP) mode $LP_{\mu\nu}$, the effective index, $n^{LP\mu\nu}$, the effective group index, $n_g^{LP\mu\nu}$ and respective the mode field distribution. The DMD of the $LP_{\mu\nu}$ mode is calculated taking the LP_{01} mode as reference and is given by $DMD_{LP\mu\nu}(\lambda) = [\bar{n}_g^{LP\mu\nu}(\lambda) - \bar{n}_g^{LP01}(\lambda)] / c$, where λ is the wavelength and c is the light velocity in vacuum. The MDL is calculated taking into account the Rayleigh scattering loss [31], the MBL [32] and coating loss [33], as described in detail further on.

The optimization function chosen (to be minimized) is given by the maximum DMD (*maxDMD*) among the guided modes and over the wavelength range given of interest, the C-band:

$$maxDMD(pv) = \max_{\lambda}\left(\max_{\mu\nu}(|DMD(\lambda,\mu\nu)|)\right). \quad (2)$$

For the optimization function (2), the search space defined by *pv* can be significantly reduced by knowing the interdependence among the *pv* elements and their relationship with key figures of merit such as the number of modes guided and their respective DMD. This is:

A. Core radius and core contrast

w_1 and Δn_{co} have the largest impact in defining the number of modes supported by a given graded-index core, the larger these are the larger the number of guided spatial modes N [34], $2N \approx V^2/4\cdot[\alpha/(\alpha+2)]$, where V is the normalized frequency $V = 2\pi w_1/\lambda \cdot [n_{co}^2 - n_{cl}^2]^{1/2}$, $n_{co} = n(0)$. Therefore, when designing a graded-index core fiber to have a given number of modes, one may choose the highest V that guarantees the guidance of the first n^{th}-modes while cutting off the next higher-order modes, as in [35]. w_1 for each target is then readily available from V, considering the lowest λ of the band of interest (C-band). However, w_1 and Δn_{co} cannot be increased indefinitely. The fiber cladding cannot be wider than 125μm for mechanical reliability. And the larger Δn_{co} becomes, the larger the DMD and the Rayleigh scattering loss (given the larger Ge doping concentration). Note that, the larger the Δn_{co}, the larger the difference $|n^{LP\mu\nu} - n^{LP01}|$ and so $|n_g^{LP\mu\nu} - n_g^{LP01}|$ becomes, i.e., DMD, since $n_g^{LP\mu\nu} = n^{LP\mu\nu} + \lambda\cdot[dn^{LP\mu\nu}/d\lambda]$. The trade-off between the number of modes and the levels of DMD and MDL will be further analyzed in Section III.

B. Core grading index and cladding trench depth

α and Δn_{tr} mainly impact DMD. In [19], it was shown for a fiber with 3 spatial modes (LP_{01}, LP_{11a} and LP_{11b}), that α allows controlling the *DMD* average while Δn_{tr} allows controlling the *DMD* slope. Further results here for a larger number of modes lead to the same conclusions. Given that both α and Δn_{tr} have a significant impact on DMD, it is expectable that to some extent they are inter-dependent. In [19], it was shown that *maxDMD* given by (3) has a convex dependency on (α, Δn_{tr}) for a given (Δn_{co}, w_2, w_3), and again, further results here have shown that such dependency holds for the number of modes covered here – within the domains defined in (4)-(9). Finally, iterative search algorithms can be used for (α, Δn_{tr}), since *maxDMD* given by (3) has a convex dependency on such parameters.

III. Fiber Profile Optimization

The optimization algorithm and domain search are informed by the profile characteristics analyzed in the previous section. The guided mode characteristics for each solution waveguide defined by *pv* are found using the vector finite difference mode solver developed in [29] with a grid step of 0.1μm and a grid size of $4\cdot(w_1+w_2+w_3)$. Note that each $LP_{\mu\nu}$ with $\mu > 0$ is counted as two-modes also referred to as two spatial modes.

A. *Optimization algorithm*

To find the best *pv* set, knowing that *maxDMD* is a convex function of (α, Δn_{tr}) – see Section II-B, a 2D golden section search (GSS) [36] is applied over (α, Δn_{tr}) while a coarse exhaustive search (ES) is performed over (Δn_{co}, w_2, w_3). The 2D-GSS is implemented as two 1D-GSS, one over α and another over Δn_{tr}, arranged as:

$$maxDMD(\Delta n_{co}, w_2, w_3)|_{optimum} = \min_{\alpha,\Delta n_{tr}}\left(maxDMD(pv)\right) = GSS\left(\Delta n_{tr}^{-}, \Delta n_{tr}^{+}, GSS\left(\alpha^{-}, \alpha^{+}, maxDMD(pv)\right)\right) \quad (3)$$

The 2D-GSS optimizes α and Δn_{tr} with a termination tolerance on Δn_{tr} of 10^{-4} and on α of 10^{-3}. The ES optimizes the Δn_{co}, w_2 and w_3 with steps of $5{\cdot}10^{-3}$, 0.25 µm and 0.5 µm, respectively. Further reducing these tolerances by a factor of 2 changed the optimized *maxDMD* negligibly.

B. *Search domain*

The optimization search (3) is subject to different sets of constraints for each parameter:

$$\Delta n_{co} \cdot 100 \in \{1:\ 0.5:\ 4\} \quad (4)$$

$$(\alpha^{-} = 1.9) \le \alpha \le (\alpha^{+} = 2.1) \quad (5)$$

$$(\Delta n_{tr}{}^{-} = -0.04) \le \Delta n_{tr} \le (\Delta n_{tr}{}^{+} = 0) \quad (6)$$

$$w_2 \in \{0:\ 0.25:\ 3\}\mu m \quad (7)$$

$$w_3 \in \{0:\ 0.5:\ 10\}\mu m \quad (8)$$

$$(\lambda^{-} = 1530\ \text{nm}) \le \lambda \le (\lambda^{+} = 1565\ \text{nm}) \quad (9)$$

The upper limit on Δn_{co} (4) takes into account the difficulties of manufacturing Δn_{co} larger than 0.03 [37]. The range in (5) allows for wide deviations from a parabolic profile. The trench depth (6) lower limit goes beyond some of the extreme Δn_{tr} values in literature, e.g., $\Delta n \approx$ -0.02 using the PCVD process in [38], to allow for a sufficiently unconstrained search and identify an unclipped trend for Δn_{tr} with w_1 and Δn_{co} – albeit manufacturing beyond -0.01 being challenging [39]. Nevertheless, it will be shown further on, in Fig. 3 (b), that best profiles for $w_1 \gtrsim 30$ µm all have $\Delta n_{tr}^{(opt)} \lesssim$ -0.02 – for smaller w_1, quasi-optimum DMD can be obtained with $\Delta n_{tr} \lesssim$ -0.02 but with a different trench position and width. The upper limit in (7) considers that further away trenches would have reduced impact on the core modes, unless deeper trenches were possible, while for (8) it has been observed that wider trenches bring little benefit while making the fabrication more complex. (9) bounds λ to the C-band. Finally, during optimization, the total diameter $2{\cdot}(w_1{+}w_2{+}w_3)$ is limited to be compatible with a 125µm cladding – for mechanical reliability equivalent to that of standard optical fibers.

C. *DMD results*

Fig. 2 shows *maxDMD* as defined in (2) as a function of the number of guided spatial modes for several Δn_{co} – full lines for the results considering (3)-(9) – dashed lines correspond to analytical approximations derived later in this section. It can be seen (from the full lines) that larger Δn_{co} allows supporting an increasingly larger number of modes (bounded by a 125µm cladding) but at the cost of a higher *maxDMD*, as expected. However, for each Δn_{co}, and with increasing number of modes,

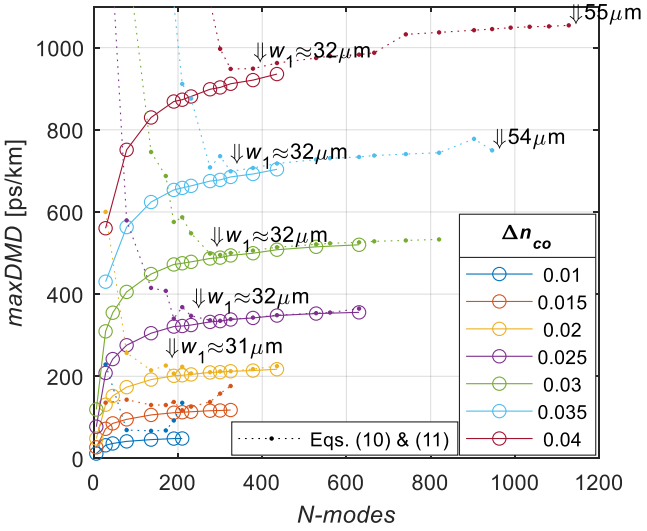

Fig. 2. *maxDMD* [ps/km] optimum values as a function of Δn_{co} for different numbers of spatial modes. Due to limited computational effort not full optimization results beyond 630 modes ('o'-markers) – only results given design rules (10) and (11) ('.'-markers).

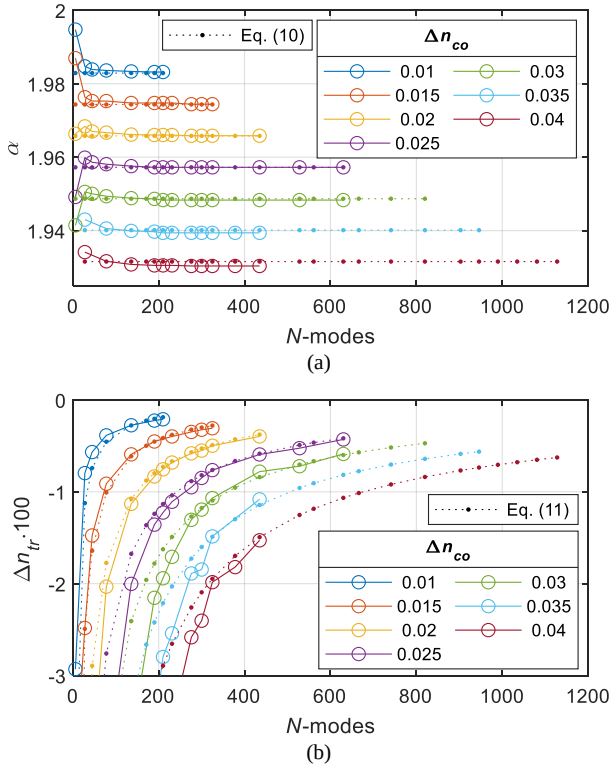

Fig. 3. Optimum fibers characteristics as a function of Δn_{co} for different numbers of spatial modes (i.e. w_1): (a) α, and (b) Δn_{tr}. Due to limited computational effort not full optimization results beyond 630 modes ('o'-markers) – only results given design rules (10) and (11) ('.'-markers).

maxDMD is found to scale quickly before levelling out as the radius of the core becomes larger than 30 µm – similar observation in [23] for $\Delta n_{co} \approx 0.01$. Therefore, at least *maxDMD*-wise, and for a given number of target modes, one should use the combination with the largest w_1 and lowest Δn_{co} that allows for the number of modes being targetted. Also from Fig. 2, one can note that over 435 spatial modes and 630 spatial modes can be supported with <250 ps/km and <450 ps/km,

respectively – 250 ps/km is typical of conventional OM fibres at 850 nm and 450 ps/km relates with the 55 spatial modes used for 1.5 Petabit/s experimental transmission in [24]. This is, provided fabrication tolerances allow, see Section V.

Analyzing the optimized *pv* sets corresponding to the results in Fig. 2 (full lines) allows concluding that w_2 = 2 μm and w_3 = 6 μm are quasi-optimal solutions, and critically, for which closed-form expressions on α and Δn_{tr} can be approximated. Fig. 3 shows the optimum profile parameters as a function of Δn_{co} for different numbers of spatial modes (i.e. w_1): (a) profile α, full lines for the results considering (3)-(9); (b) profile Δn_{tr}, full lines for the results considering (3)-(9) except for keeping fixed w_2 = 2 μm and w_3 = 6 μm. Note that, in the latter, w_2 and w_3 are hold at specific values in the interest of establishing a Δn_{tr} design trend, since many different trench dimensioning combinations lead to similar *maxDMD*. From Fig. 3-(a) (full lines) it can be seen that α is mostly defined by Δn_{co} except for small number of modes. α dependence can be approximated as:

$$\alpha^{(\text{quasi-opt})}(\Delta n_{co}) \approx 2\cdot(1 - 0.85\cdot\Delta n_{co}) \qquad (10)$$

Equation (10) follows the same principles of the scaling law derived in [34, 40]. However, the scaling slope with Δn_{co} differs since most assumptions in [34, 40] are not fully met here (e.g., w_1 is not several 100x larger than the λ). From Fig. 3-(b) (full lines), it can be seen that Δn_{tr} scales with both w_1 and Δn_{co}. Δn_{tr} dependence can be approximated as:

$$\Delta n_{tr}^{(\text{quasi-opt})}(w_1, \Delta n_{co}) \approx -0.3\cdot(75/w_1[\mu\text{m}])^2\cdot\Delta n_{co} \qquad (11)$$

Critically, in Fig. 2, the dotted lines show *maxDMD* for the profiles given by (10) and (11). It can be seen that the *pv* given by (10) and (11) are quasi-optimum for $w_1 \gtrsim 30$ μm – (10) does not cover for smaller w_1 cases. As highlighted above, when designing for a given number of modes, *maxDMD* is minimized by choosing the combination of largest w_1 and smallest Δn_{co} possible: which corresponds to the range of validity for (10) and (11).

D. Rayleigh scattering, MBL and coating loss

Now, onto fiber characteristic that induce fundamental loss of throughput. Rayleigh scattering loss is estimated using the Rayleigh scattering coefficients in [31], function of the relative refractive index difference, and integrating over the mode field distribution of each mode solution of a given fiber profile. MBL is estimated using the method in [32] that calculates the power radiated along a bend by approximating the mode field outside of the fiber in terms of a superposition of cylindrical outgoing waves and matching it to the mode field of the fiber along the cladding outer surface. Coating loss was estimated by considering a finite cladding region (125μm diameter) surrounded by a loss layer with an imaginary component added to the refractive index following the approach in [33]. In this way, the imaginary part of each mode's effective mode index corresponds to the confinement losses.

Rayleigh scattering has been found to scale with Δn_{co} given the Ge-doping increase. Fig. 4 shows Rayleigh scattering as a function of the number of spatial modes for the optimized fibers in Fig. 2. The difference in Rayleigh scattering loss between the best and worst mode is mainly defined by Δn_{co}, at least for >100 spatial modes, approaching 0.1 dB/km for Δn_{co} = 0.03.

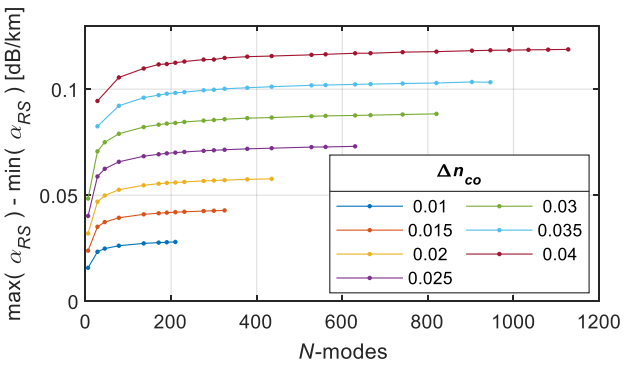

Fig. 4. Rayleigh scattering loss as a function of the number of spatial modes for the best fibers in Fig. 2 (i.e., best fibers between those obtained with (3) and those obtained with (10)&(11), as available).

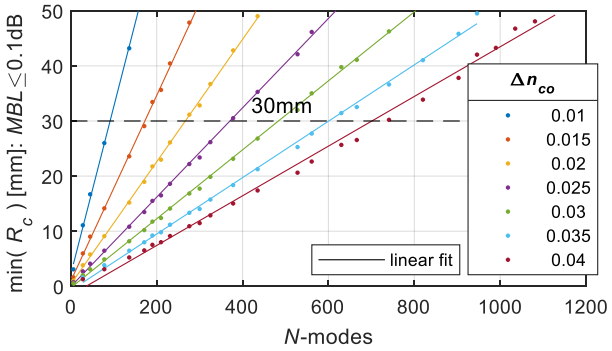

Fig. 5. Average min(R_c) in the 2nd to last mode group as a function of the number of spatial modes – for all the best cases in Fig. 2 (i.e., best between (3) and (10)&(11), as available).

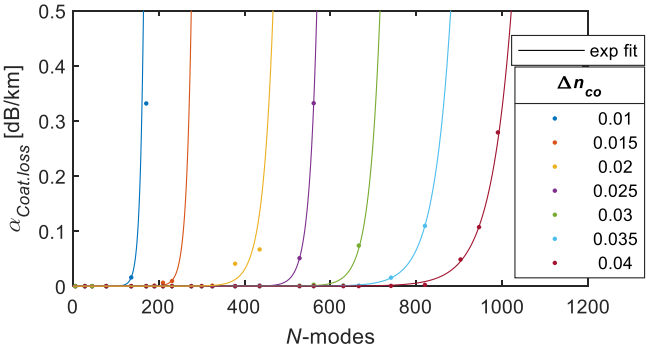

Fig. 6. Average coating loss in the 2nd to last mode group as a function of the number of spatial modes for the best fibers shown in Fig. 2 (i.e., best between (3) and (10)&(11), as available).

Fig. 5 shows minimum radius of curvature min(R_c), such that for 100 turns *MBL* < 0.1 dB at 1625 nm, as a function of the number of spatial modes the optimized fibers in Fig. 2. Note that it is the average min(R_c) in the 2nd to last mode group that is plotted – following the approach in [23], the average min(R_c) in the last mode group was found to vary too widely to offer insight here. From Fig. 5, it can be seen that min(R_c) tends to increase with the number of modes for a given Δn_{co} and that the slope of such scaling decreases significantly for larger Δn_{co}. Nevertheless, reaching values comparable to or above that of SMFs (i.e., 30 mm). Note that, for a given Δn_{co}, the more mode groups are forced into a given Δn_{co} range (by increasing w_1), the closer the effective mode indexes in the higher order groups

become to the effective indexes of radiation modes, hence an increase of the *MBL* in the higher order groups with w_1.

Allowing for larger cores than in conventional fibers can make the coating loss of the fiber increase [27]. For larger core diameters, the evanescent field (in particular, of higher order modes) can have significant amplitudes at the cladding-coating boundary leading to excess loss. Following the method in [33], the coating loss is directly estimated from the imaginary part of the effective index obtained given a perfectly matched layer. Fig. 6 shows the average coating loss for the 2nd to last mode group as a function of the number of spatial modes for the optimized fibers in Fig. 2. It can be seen that for all Δn_{co}, coating loss becomes significant as the profile outer dimensions approach the cladding diameter, 125 µm. For example, for $\Delta n_{co} = 0.03$, coating loss becomes significant beyond 600 spatial modes.

The combined impact of Rayleigh scattering loss, MBL and coating loss on to the throughput scaling with the number of modes is studied in Section IV.

IV. Coupled Transmission and Channel Throughput

In this section, the achievable throughput for the optimized fibers in Section III is analyzed. Given the fiber transfer matrix $H[f]$, the achievable throughput is estimated from MIMO theory using the water filling algorithm [41].

The channel transfer function $H[f]$ for each optimized fiber is calculated for a single span of 100 km using the multi-section model in [17] and considering a section-size of 10 m. For a $2N$ polarization mode fiber and a set of N_f frequencies, $H[f]$ becomes a $2N\times2N\times N_f$ matrix. A $N_f = 128$-long frequency vector is considered to account for the frequency dependent response along the C-band (1530-1565 nm). The calculation of H considers all main linear impairments, this is Rayleigh scattering loss and coating loss, MBL, DMD and LMC. Rayleigh scattering, coating loss and DMD are fully determined by the optimized refractive-index profile as explained before. MBL corresponding to 1 turn with a R_c of 30 mm is applied to every fiber section. And finally, random LMC corresponding to a core-cladding boundary distortion of 0.06% of the fiber radius and uniformly distributed azimuthal offset [42] is introduced every fiber section. Such core-cladding boundary imperfections are similar to that of manufactured multimode fibers [43]. Using MIMO theory [41], information throughput is computed by decomposing channel (fiber) matrix $H[f]$ into a set of parallel, independent scalar Gaussian sub-channels through a singular value decomposition (SVD). This is, $H[f] = U[f]S[f]V[f]^{\mathrm{H}}$, where U and V are unitary matrices and S is a diagonal matrix whose diagonal elements $\lambda_1^{[f]}, \ldots, \lambda_{2N}^{[f]}$ are non-negative real numbers. Each non-zero eigenmode $\lambda_i^{[f]}$ can support a data tributary, $i = 1, \ldots, n_{NZ}$. In this way, a throughput bound T, assuming full channel state information, is given by:

$$T = 5\ \mathrm{THz} / 128 \sum_{f=-64:63} \sum_{i=1:n_{NZ}} \log(1 + P_i[f]\lambda_i^2[f]/N_0) \qquad (12)$$

bits/s, where $P_1^{[f]}, \ldots, P_{n_{NZ}}^{[f]}$ are the waterfilling power allocations $P_i^{[f]} = (\mu + N_0 / (\lambda_i^{[f]})^2)^+$ for frequency channel f, with μ chosen to satisfy the total power constraint $\sum P_i^{[f]} = P$, and $(\cdot)^+$ is zero if its argument is negative. We choose N_0 such

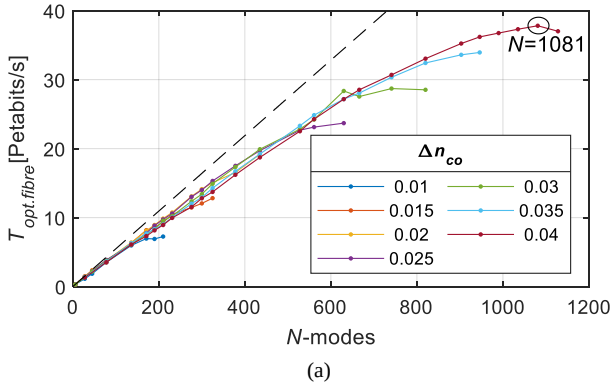

(a)

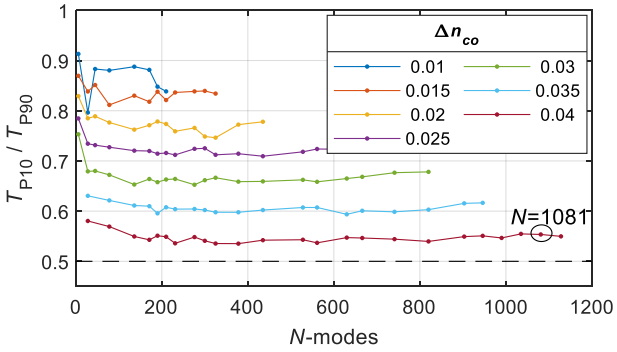

(b)

Fig. 7. Throughput as a function of the number of spatial modes for several Δn_{co}, same optimized fibers as in Fig. 2. (a) total throughput, and (b) ratio between the average throughput per mode of the 10th-percentile and that of the 90th-percentile.

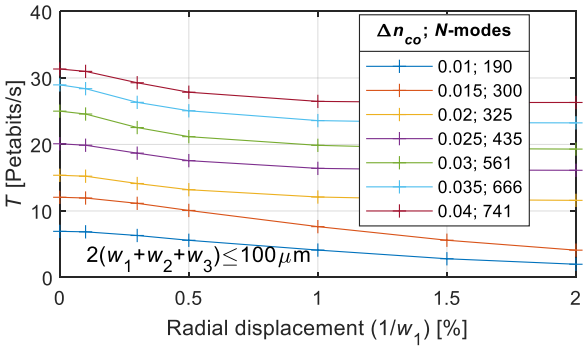

(a)

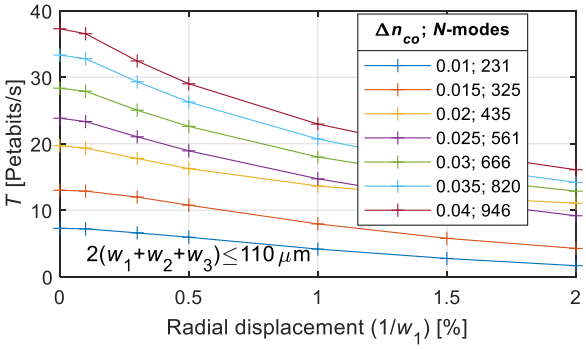

(b)

Fig. 8. Throughput as a function of the radial offset for the optimized fibre with largest number of spatial modes at each Δn_{co} level in Fig. 2, considering: (a) $2(w_1+w_2+w_3) \leq 100$µm and (b) $2(w_1+w_2+w_3) \leq 110$µm.

that the lowest loss mode has a signal-to-noise (SNR) of 17 dB which is compatible with 100 km transmission in a power-limited

scenario.

Fig. 7 (a) shows throughput as a function of the number of spatial modes for several Δn_{co} – same optimum fibers of Fig. 2. It can be seen that, in principle, a throughput in excess of 35 Petabit/s can be reached (several times larger than the 1.5 Petabit/s over the optimized 55 spatial modes MMF in [24]). However, the spatial multiplexing gain deviates from a 1-to-1 linear gain given the increase in MDL – driven in first instance by Rayleigh scattering loss. Note that MDL scales with the number of modes, as explained in Section III-D. Also, in Fig. 7 (a), it can be seen that throughput can decrease with *N*-modes after peaking for a large *N*, specifically, $N = 1081$ at $\Delta n_{co} = 0.04$. This corresponds to $2\cdot(w_1+w_2+w_3) \approx 125$ µm, in which case MBL and coating loss become dominant even for the 2nd to last mode group, Fig. 5 and Fig. 6.

Fig. 7 (b) shows the ratio between the average throughput per mode for the 10th percentile and that of the 90th percentile. Interestingly, the percentile ratio remains constant when increasing *N*-modes for a given Δn_{co}, indicating that MDL induced by Rayleigh scattering is the main mechanism for degradation on relative throughput per mode. Furthermore, from Fig. 7 (b), it can be inferred that beyond $\Delta n_{co} = 0.04$, the additional throughput per added mode has been halved. The number of modes leading to the largest throughput (in Fig. 7 (a)) within this relative threshold ($T_{10}/T_{90} \approx 0.5$ in Fig. 7 (b)), we dub here as the half-mode number of graded-index multimode fibers, namely $N = 1081$ at $\Delta n_{co} = 0.04$. The half-mode number is a useful metric since it may be more efficient, cost- and energy-wise, to operate with a smaller Δn_{co} and a smaller *N*-modes but with larger throughput per mode. Note that this *half-mode number* can increase with the SNR available to resolve the highest loss modes, or vice-versa.

Finally, we analyze the throughput of the optimized fibers discussed above for increasing linear coupling strength. Fig. 8 shows throughput as a function of the radial displacement for several Δn_{co} and respective maximum number of spatial modes in Fig. 2, for: (a) $2\cdot(w_1+w_2+w_3) \leq 100$µm and (b) $2\cdot(w_1+w_2+w_3) \leq 110$µm. The throughput can be seen decreasing with the radial displacement (i.e., linear mode coupling strength). In Fig. 8 (a), the total throughput degradation is relatively small ≲20%. However, for the wider profiles in Fig. 8 (b), the degradation is more pronounced, approaching 60% loss in the total throughput for stronger linear mode coupling. Note that, although linear mode coupling can decrease the standard deviation of the overall MDL, it can also increase the average loss. Here, linear mode coupling is spreading the significant MBL and coating loss of the two last mode groups (Fig. 5 and Fig. 6) into further lower order mode groups, reducing the total number of modes viable for transmission at a given SNR. From Fig. 8 (a) and (b), it can be concluded that there is no benefit in going for fiber profiles wider than 100 µm – in line with Fig. 7 (a).

V. MANUFACTURING MARGINS

The optimized parameters in Section III were obtained ignoring the finite precision of the manufacturing processes. Fabrication limitations lead to the deviation of the manufactured fiber parameters from the optimum values, causing *maxDMD* to increase. According to [44], profile deviations are well described by normal distributions with a given standard deviation σ. We investigate the impact of profile distortions reported for MMFs of category OM3. In [37], the measurements reported indicated a σ for Δn ($\sigma_{\Delta n}$) around $5\cdot10^{-5}$ and a σ for the layers widths (σ_w) around 1 %. Here, we consider $\sigma_{\Delta n} = 10^{-4}$ and $\sigma_w = 0.01\cdot w$.

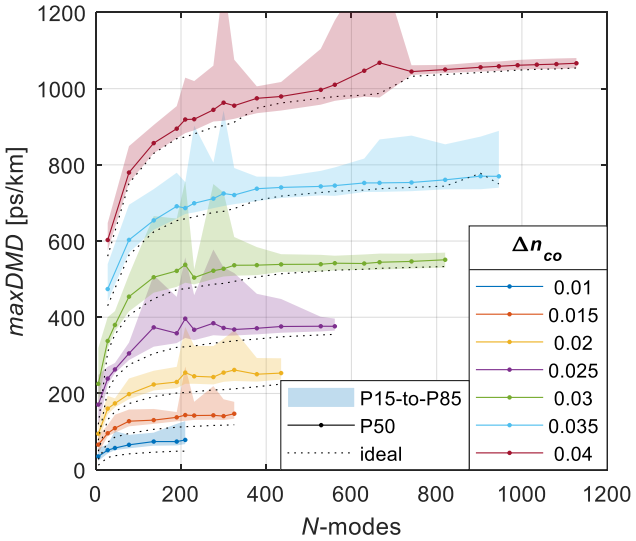

Fig. 9. *maxDMD* as a function of the number of spatial modes in the presence of fabrication deviations on the profile layers width. Highlighted areas correspond to the range between the 15th-percentile and the 85th-percentile for 100 different profile distortion realizations.

Fig. 9 shows *maxDMD* as a function of the number of spatial modes for the Δn_{co} values considered before. The 15th-, 50th- and 85th-percentile for 100 different profile distortion realizations given $\sigma_{\Delta n}$ and σ_w are presented. Each profile distortion realization includes: an independent perturbation to the width of each of the three layers (w_1, w_2, w_3) following a normal distribution with $\sigma_{wi} = 0.01\cdot w_i$; an independent perturbation to the Δn value in each step of the mode solver grid, following a normal distribution with $\sigma_{\Delta n} = 10^{-4}$. It can be seen from Fig. 9 that some of the optimized profiles are more vulnerable to distortions than others. This could be expected since resilience to distortion is not part of the optimization function in (2). Fig. 9 also shows some areas where the distorted profile performs marginally better than the ideal optimized profile in Fig. 2. These correspond to the cases in Fig. 2 containing results only for Eqs. (10) and (11), i.e., no full optimization results available with (3). Moreover, note the small *maxDMD* deviations for large number of modes and $\Delta n_{co} = 0.03$ or $\Delta n_{co} = 0.04$ – it suggests that including resilience to distortion in (2) can indeed be a valid approach.

In general, and excluding the optimized profiles with *maxDMD* increasing disproportionally, the results in Fig. 9 indicate that the relative *maxDMD* degradation could be tolerable. In particular, for applications using coherent detection and advanced MIMO-DSP processing (e.g., in [24], 1.5 Pb/s was transmitted in a fiber with a *maxDMD* as high as 450 ps/km). In any case, a more detailed analysis is required with specific preform and drawing tower data. Such analysis is

out of the scope of this paper, it instead focusses on the best achievable transmission characteristics.

VI. Conclusions

We have investigated the design of graded-index trench-assisted multimode fibers supporting over 1000-modes (and twice as many polarizations modes) for minimum differential mode delay in the C-band. It was shown that over 400-modes can be supported within a maximum differential mode delay of 250 ps/km, typical of OM fibers at 850 nm. And that, for a given core-cladding contrast, the number of modes can be scaled by increasing the core radius without significant degradation of the differential mode delay. Importantly, closed-form equations for optimal profile parameters are introduced, function only of the core radius and the core-cladding contrast. Also, the fabrication margins were found to have a significant but manageable impact on the mode delay of the optimized profiles, a *maxDMD* degradation smaller than 15 % in many of the cases.

We identified the scaling trend with the number of modes for several trade-offs such as those imposed by Rayleigh scattering, MBL, coating loss, and linear mode coupling. We have quantified how these effects limit throughput and found the number of spatial modes beyond which added throughput per mode is halved, $N = 1081$ – which we dubbed as the *graded-index multimode fibers half-mode number*. Allowing for the transmission of as much as 35 Petabits/s over 100 km, assuming *SNR* ~17dB. In doing so, it has been concluded that for fiber profiles wider than 100 μm, throughput can actually decrease, and that for refractive-index contrasts beyond 0.04, throughput scaling enters a strong diminishing returns regime.

The findings presented here make it possible to identify operational regimes for multimode fibers maximizing their potential to provide much wider conduits of information in future high-throughput SDM transmission systems.

References

[1] D. J. Richardson, J. M. Fini, and L. E. Nelson, "Space-division multiplexing in optical fibres," *Nature Photonics*, vol. 7, p. 354, 2013, doi: 10.1038/nphoton.2013.94.

[2] P. Sillard, D. Molin, M. Bigot-Astruc, A. Amezcua-Correa, K. d. Jongh, and F. Achten, "50 μm Multimode Fibers for Mode Division Multiplexing," *Journal of Lightwave Technology*, vol. 34, no. 8, pp. 1672-1677, 2016, doi: 10.1109/JLT.2015.2507442.

[3] M. J. Li *et al.*, "Multicore Multimode Fiber-A New Type of Fiber Using Coupled-Core Structures," *IEEE Journal of Selected Topics in Quantum Electronics*, vol. 26, no. 4, pp. 1-10, 2020, doi: 10.1109/JSTQE.2020.2969564.

[4] K. Li, X. Chen, A. R. Zakharian, J. E. Hurley, J. S. Stone, and M.-J. Li, "Large core multimode fiber with high bandwidth and high connector tolerance for broadband short distance communications," *APL Photonics*, vol. 6, no. 7, p. 070802, 2021/07/01 2021, doi: 10.1063/5.0056669.

[5] L. Gruner-Nielsen *et al.*, "Few Mode Transmission Fiber With Low DGD, Low Mode Coupling, and Low Loss," *J. Light. Technol.*, vol. 30, no. 23, pp. 3693-3698, 2012, doi: 10.1109/jlt.2012.2227243.

[6] T. Hayashi, T. Taru, O. Shimakawa, T. Sasaki, and E. Sasaoka, "Design and fabrication of ultra-low crosstalk and low-loss multi-core fiber," *Optics Express*, vol. 19, no. 17, pp. 16576-16592, 2011/08/15 2011, doi: 10.1364/OE.19.016576.

[7] B. Zhu *et al.*, "Seven-core multicore fiber transmissions for passive optical network," *Optics Express*, vol. 18, no. 11, pp. 11117-11122, 2010/05/24 2010, doi: 10.1364/OE.18.011117.

[8] C. Antonelli and A. Mecozzi, "Near-Zero Modal-Dispersion (NEMO) Coupled-Core Multi-Core Fibers," *Journal of Lightwave Technology*, vol. 39, no. 23, pp. 7517-7528, 2021, doi: 10.1109/JLT.2021.3115912.

[9] T. Hayashi *et al.*, "Randomly-Coupled Multi-Core Fiber Technology," *Proceedings of the IEEE*, vol. 110, no. 11, pp. 1786-1803, 2022, doi: 10.1109/JPROC.2022.3182049.

[10] M. D. Feuer *et al.*, "Joint Digital Signal Processing Receivers for Spatial Superchannels," *IEEE Photonics Technology Letters*, vol. 24, no. 21, pp. 1957-1960, 2012, doi: 10.1109/LPT.2012.2220672.

[11] B. Inan *et al.*, "DSP complexity of mode-division multiplexed receivers," *Opt. Express*, vol. 20, no. 10, p. 10859, 2012, doi: 10.1364/OE.20.010859.

[12] A. Lobato *et al.*, "Impact of mode coupling on the mode-dependent loss tolerance in few-mode fiber transmission," *Opt. Express*, vol. 20, no. 28, p. 29776, 2012, doi: 10.1364/OE.20.029776.

[13] F. Ferreira, P. Monteiro, and H. Silva, "Semi-analytical model for linear modal coupling in few-mode fiber transmission," in *Proc. ICTON*, 2012, p. Th.A1.5, doi: 10.1109/icton.2012.6254446.

[14] K.-P. Ho and J. M. Kahn, "Linear Propagation Effects in Mode-Division Multiplexing Systems," *J. Light. Technol.*, vol. 32, no. 4, pp. 614-628, 2014, doi: 10.1109/jlt.2013.2283797.

[15] A. Mecozzi, C. Antonelli, and M. Shtaif, "Intensity impulse response of SDM links," *Opt. Express*, vol. 23, no. 5, pp. 5738-43, 2015, doi: 10.1364/OE.23.005738.

[16] C. Antonelli, A. Mecozzi, and M. Shtaif, "The delay spread in fibers for SDM transmission: dependence on fiber parameters and perturbations," *Opt. Express*, vol. 23, no. 3, pp. 2196-202, 2015, doi: 10.1364/OE.23.002196.

[17] F. M. Ferreira, C. S. Costa, S. Sygletos, and A. D. Ellis, "Semi-Analytical Modelling of Linear Mode Coupling in Few-Mode Fibers," *J. Light. Technol.*, vol. 35, no. 18, pp. 4011-4022, 2017, doi: 10.1109/jlt.2017.2727441.

[18] J. Vuong, P. Ramantanis, A. Seck, D. Bendimerad, and Y. Frignac, "Understanding discrete linear mode coupling in few-mode fiber transmission systems," in *Proc. ECOC*, 2011, p. Tu.5.B.2.

[19] F. Ferreira, D. Fonseca, and H. J. A. Silva, "Design of few-mode fibers with M-modes and low differential mode delay," *Journal of Lightwave Technology*, vol. 32, no. 3, pp. 353--360, 2 2014, doi: 10.1109/JLT.2013.2293066.

[20] F. Ferreira, D. Fonseca, and H. Silva, "Design of few-mode fibers with arbitrary and flattened differential mode delay," *IEEE Photonics Technology Letters*, vol. 25, no. 5, pp. 438--441, 2 2013, doi: 10.1109/LPT.2013.2241047.

[21] M. J. Li, X. Chen, A. R. Zakharian, J. E. Hurley, and J. S. Stone, "Large Core Multimode Fiber for Short Distance Communications," in *2022 27th OptoElectronics and Communications Conference (OECC) and 2022 International Conference on Photonics in Switching and Computing (PSC)*, 3-6 July 2022 2022, pp. 1-3, doi: 10.23919/OECC/PSC53152.2022.9849917.

[22] G. Rademacher, "Randomly Coupled 19-core Multi-Core Fiber with Standard Cladding Diameter," in *OFC*, 2023, p. Th4A.4.

[23] P. Sillard, D. Molin, M. Bigot-Astruc, K. d. Jongh, and F. Achten, "Rescaled Multimode Fibers for Mode-Division Multiplexing," *Journal of Lightwave Technology*, vol. 35, no. 8, pp. 1444-1449, 2017, doi: 10.1109/JLT.2017.2657005.

[24] G. Rademacher, "1.53 Peta-bit/s C-Band Transmission in a 55-Mode Fiber," *ECOC*, p. Th3C.3, 2022.

[25] J.-i. Sakai and T. Kimura, "Bending loss of propagation modes in arbitrary-index profile optical fibers," *Appl. Opt.*, vol. 17, no. 10, pp. 1499-1506, 1978/05/15 1978, doi: 10.1364/AO.17.001499.

[26] W. Zhi, R. Guobin, L. Shuqin, and J. Shuisheng, "Loss properties due to Rayleigh scattering in different types of fiber," *Optics Express*, vol. 11, no. 1, pp. 39-47, 2003/01/13 2003, doi: 10.1364/OE.11.000039.

[27] K. Takenaga *et al.*, "A large effective area multi-core fiber with an optimized cladding thickness," *Optics Express*, vol. 19, no. 26, pp. B543-B550, 2011/12/12 2011, doi: 10.1364/OE.19.00B543.

[28] Y. Sun *et al.*, "Advanced multimode fiber for high-speed short-read interconnect," 2008/11/1, vol. 7134, p. 71341L.

[29] A. B. Fallahkhair, K. S. Li, and T. E. Murphy, "Vector Finite Difference Modesolver for Anisotropic Dielectric Waveguides," *Journal of Lightwave Technology*, vol. 26, no. 11, pp. 1423-1431, 2008, doi: 10.1109/JLT.2008.923643.

[30] W. Hermann and D. U. Wiechert, "Refractive index of doped and undoped PCVD bulk silica," *Materials Research Bulletin*, vol. 24, pp. 1083-1097, 1989.
[31] M. Ohashi, K. Shiraki, and K. Tajima, "Optical loss property of silica-based single-mode fibers," *Journal of Lightwave Technology*, vol. 10, no. 5, pp. 539-543, 1992, doi: 10.1109/50.136085.
[32] K. S. Kaufman, R. Terras, and R. F. Mathis, "Curvature loss in multimode optical fibers," *J. Opt. Soc. Am.*, vol. 71, no. 12, pp. 1513-1518, 1981/12/01 1981, doi: 10.1364/JOSA.71.001513.
[33] K. Saitoh and M. Koshiba, "Full-vectorial imaginary-distance beam propagation method based on a finite element scheme: application to photonic crystal fibers," *IEEE Journal of Quantum Electronics*, vol. 38, no. 7, pp. 927-933, 2002, doi: 10.1109/JQE.2002.1017609.
[34] D. Gloge and E. A. J. Marcatili, "Multimode theory of graded-core fibers," *The Bell System Technical Journal*, vol. 52, no. 9, pp. 1563-1578, 1973, doi: 10.1002/j.1538-7305.1973.tb02033.x.
[35] M. Bigot-Astruc, D. Boivin, and P. Sillard, "Design and fabrication of weakly-coupled few-modes fibers," in *2012 IEEE Photonics Society Summer Topical Meeting Series*, 9-11 July 2012 2012, pp. 189-190, doi: 10.1109/PHOSST.2012.6280766.
[36] W. H., S. Teukolsky, W. Vetterling, and B. Flannery, *Numerical Recipes 3rd Edition: The Art of Scientific Computing*. 2007.
[37] A. V. Bourdine, "Design of Refractive Index Profile for Multimode Optical Fibers with Low Differential Mode Delay," *Journal of Optoelectronics Engineering*, vol. 1, no. 1, pp. 5-13, 2013/09/10 2013, doi: 10.12691/joe-1-1-2.
[38] P. Bachmann, P. Geittner, D. Leers, and H. Wilson, "Loss reduction in fluorine-doped SM- and high N.A.-PCVD fibers," *Journal of Lightwave Technology*, vol. 4, no. 7, pp. 813-817, 1986, doi: 10.1109/JLT.1986.1074805.
[39] A. E. Miller, R. L. Opila, and M. F. Yan, "Ultranegative delta cladding for modified chemical vapor deposition," in *Optical Fiber Communications, OFC.*, 25 Feb.-1 March 1996 1996, pp. 56-58, doi: 10.1109/OFC.1996.907638.
[40] R. Olshansky and D. B. Keck, "Pulse broadening in graded-index optical fibers," *Appl. Opt.*, vol. 15, no. 2, pp. 483-491, 1976/02/01 1976, doi: 10.1364/AO.15.000483.
[41] D. Tse and P. Viswanath, *Fundamentals of Wireless Communication*. Cambridge: Cambridge University Press, 2005.
[42] F. M. Ferreira, C. S. Costa, S. Sygletos, and A. D. Ellis, "Semi-analytical modelling of linear mode coupling in few-mode fibers," *Journal of Lightwave Technology*, 7 2017, doi: 10.1109/JLT.2017.2727441.
[43] A. Bourdine, D. Praporshchikov, and K. Yablochkin, *Investigation of defects of refractive index profile of silica graded-index multimode fibers* (Optical Technologies for Telecommunications 2010). SPIE, 2011.
[44] P. H. Krawarik and L. S. Watkins, "Fiber geometry specifications and its relation to measured fiber statistics," *Appl. Opt.*, vol. 17, no. 24, pp. 3984-3989, 1978/12/15 1978, doi: 10.1364/AO.17.003984.